UNIVERSITÀ DI PISA

Faculty of Engineering

Bachelor of Science in Computer Engineering

A WTA COMPETITIVE LEARNING ALGORITHM FOR THE DEVELOPMENT OF CORTICAL RECEPTIVE FIELDS

Thesis Supervisors:

Prof. M. C. CARROZZA

Prof. M. PAPPALARDO

Prof. G. VAGLINI

Author:

GIACOMO SPIGLER

December, 2012

ABSTRACT

This thesis investigates the problem of modeling the learning of cortical receptive fields through competitive interaction mediated by local winner take all operations. Given the great amount of data about the Primary Visual Cortex V1, such cortical area is used for a meaningful comparison of the physiological responses and the shape of the learnt receptive fields. The learning algorithm we developed is based on the basic Oja learning rule, but convergence to different weight vectors is enforced by local competition.

ACKNOWLEDGMENTS

I would like to thank all my friends, with whom I shared so many wonderful experiences. A big thanks is deserved by Valerio, for the hilarious times he surely remembers, by FruFFri (aka Francesca), for everything in the past three years, and by Niccolo', for the university and life experiences.

I am extremely grateful to Scuola Sant'Anna and all the people and friends I've met there, who accompanied me in the past three years and with whom in those years I shared most of my life. Another thanks goes to my high school professors at Liceo Newton, who guided me through a personal growth and could appreciate my proactivity.

The biggest thanks is for my parents, who always supported me and gave me countless opportunities to travel, study and learn, and they taught me the value of work and education.

Last but not least, I owe a special thanks to Dr. Calogero Oddo and Prof. Maria Chiara Carrozza for their critical help in reviewing this Thesis.

Pisa, 26^{th} November

TABLE OF CONTENTS

CHAPTER 1

INTRODUCTION

The main motivation behind our work stems from the need for computational models inspired by the biological brains to improve the quality of real world applications. For this reason, we can somehow point out a difference in comparison to classical computational neuroscience, in that we are mostly interested in studying the workings of biological nervous systems, with great emphasis on the neocortex, to be able to produce fast and reliable applications in order to improve the perceptual and cognitive abilities of artificial machines. Because of this, in our entire text we are focused on the possibility of real world applications of the systems we present.

In particular, we tackle the problem of developing a computational model to reproduce some of the dynamics of the neocortex by studying how the mammal visual system works, given the huge amount of data in that field, at quite some levels of abstraction and detail, and the existence of many different models in literature to compare with. In this context, we used the Caltech101 image database [12] to provide input to the our model, which was implemented in C++, and after running our simulations we validated the computed parameters in comparison to the biological receptive fields of neurons in Primary Visual Cortex (both through visual inspection and by fitting Gabor filters).

This thesis is organized as a brief review of the topics most relevant to this work, along with the description of related state-of-the-art models. Following in Chapter 3 we present our main contribution, and we discuss its problems and advantages concluding the text in Chapter 4.

CHAPTER 2

BACKGROUND

We begin with a quick review of the main concepts in neuroscience that are required for the scope of this work, and we present some models which are the state of the art of the problem being discussed.

2.1 Biology

In this brief summary, we begin from the most basic elements of biological Nervous Systems, the neurons. We then identify more complex building blocks of the mammalian Neocortex, identifying its structure and elements. At last, we conclude with a discussion about the (primate / mammal) Visual System and its parts which are most relevant for this thesis, such as cortical maps and the Primary Visual Cortex.

2.1.1 Neurons

Neurons are the basic cellular elements of the nervous system, and they are the main signaling units [19]. There have been found many types of these highly specialized cells, but all share a common morphology (see Fig. 2.1 for an example). Despite some variability, neurons usually receive signals through their Dendrites, process information and produce an output, which is transmitted by their Axon as a sequential membrane depolarization, the Action Potential.

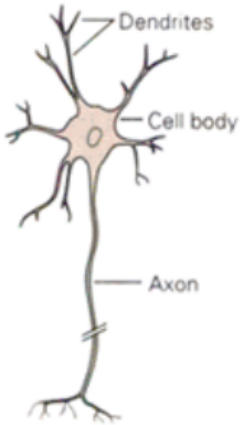

Figure 2.1: *A neuron [19].*

Even though we don't yet know all the mechanisms for neural coding of information, several have been identified, ranging from Rate coding (frequency of spikes) to Temporal coding (accounting for the precise timing at which spikes are generated) and to Population coding (single neuron output is noisy, but the joint activity of a cluster of cells can be very robust). Communication is mediated by electrochemical signals in the Synapses, special structures connecting neurons (usually, axons to dendrites). At the level of a synapse, action potentials cause the release of endogenous chemicals, the Neurotransmitters, that in turn bind with specific Receptors, which control the ion flux in the post-synaptic cell. Neurotransmitters can be Amino acids (eg, glutamate, one of the most ubiquitous, present in excitatory synapses, and GABA γ-aminobutyric acid, employed by inhibitory interneurons), Peptides or other chemicals (eg, acetylcholine).

Neuron types differ in chemical composition of the neurotransmitters they produce, in synaptic receptors and in shape (see Table 2.1 for an example). Pyramidal cells are the primary excitatory neurons in the mammalian brains, and are characterized by a triangular shaped soma (the cell body), with a single axon and a large apical dendrite, multiple basal dendrites and the presence of dendritic spines, while Double Bouquet cells get their name from their vertically organized dendritic branches, spread in two opposite directions. Moreover, Spiny Stellate cells are identified by a star-like shape and spiny dendrites, and Basket cells are common GABA-ergic inhibitory interneurons found in mammalian neocortex.

	Pyramidal	Double Bouquet	Spiny Stellate	Basket cell
Post-synaptic	excitatory	inhibitory	excitatory	inhibitory
Shape	triangular body	vertical organization	star-like shape	"basket" like
Cortical layer	II-III-V	II-III	IV C	I

Table 2.1: *Summary of the most common cortical neuron types.*

For this thesis, the most important neural dynamics is learning, that is long-term synaptic potentiation or depression, wich in practice changes the "weight" a given synapse has in making the post-synaptic neuron fire in response to the activity of the pre-synaptic one.

2.1.2 Neocortical architecture: layers, mini/macro columns

The Neocortex is the latest evolutionary improvement to mammalian brains, and is a thin layer which surrounds the rest of the brain. In humans, it has been estimated to contain around 20 billion neurons, each one connected with up to 10.000 others (for a total number in the order of 100-200 trillion synapses). The Neocortex of large mammals and primates present characteristic sulci and gyri, which have evolved to increase the overall cortical surface under the constraints of the skull's size. Its functions are related to higher level cognitive tasks, such as sensory perception and voluntary control of movement, planning, communication and thought.

Primate cortex is 2.3-2.8 millimeters thick, and is made up of 6 layers marked by differences in the morphology of neurons and their connectivity (Fig. 2.2). Despite presenting some differences in specific cortical areas (eg, Primary Motor cortex) every layer has been linked to specific functions: layer IV receives input from outside the cortex (mostly from the Thalamus) and distributes it with short range inter-layer connections implemented by the Spiny Stellate cells, while layers II / III project their axons to other cortical areas and layers V / VI project out of the cortex, to subcortical structures. Layer I has few cell bodies, and is mostly made up of axons and apical dendritic tufts. Most of the neurons are excitatory pyramidal neurons (around 80% of them), and the rest are mainly inhibitory interneurons (20%; among which Basket cells have great relevance).

Morover, besides its laminar structure, the Neocortex presents another level of organization, that is its modular architecture as a mosaic of cortical columns, which

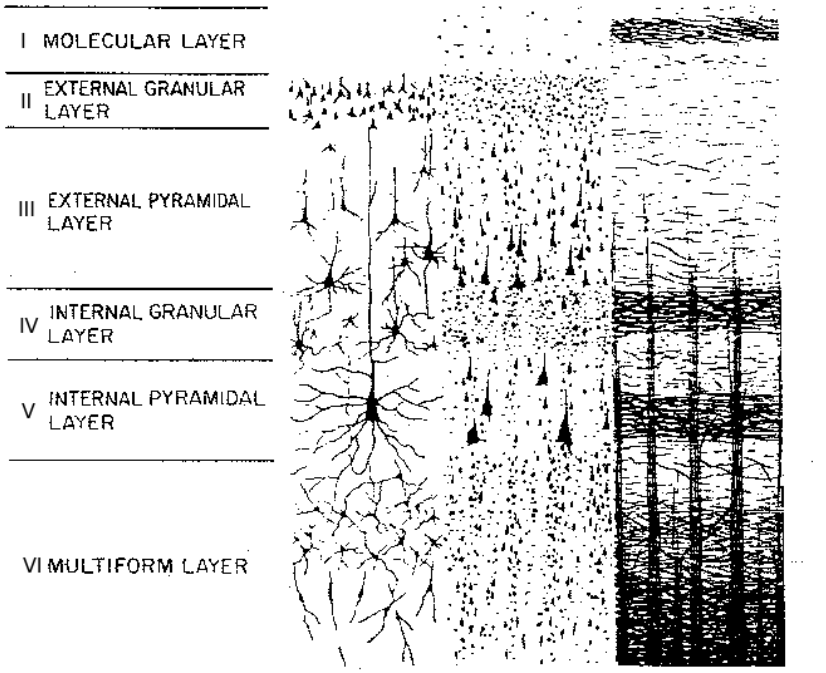

Figure 2.2: *Laminar structure of the Neocortex.*

have been proposed as the basic building blocks of cortical function [26] [7]. In fact, experiments proved that neurons aligned perpendicularly to the surface of the cortex and within a diameter of 28-40 um responded to stimuli in a very similar way, whereas the response was quite different moving tangentially. Each *minicolumn* contains 80-120 neurons on average, and is highly interconnected with neighboring columns. Also, these structures can be further grouped into *macrocolumns*, being modules inside which a full set of values for any set of receptive field parameters is found (eg, in Hubel and Wiesel IceCube model of V1, a macrocolumn contains columns selective to a full range of orientations and spatial frequencies, for both eyes). Some estimates suggest there are 50-100 minicolumns composing each macrocolumn, for a total of 4000-12000 neurons and a diameter of 200-800 um. Neurons farther apart than this length don't generally have overlapping receptive fields.

After first discovery of the cortical minicolumn in the 50s [25] a lot of research

provided evidence in support of a broad columnar organization across the cortex, with special mention deserved for sensory cortices [18] [10] [11], motor cortex, IT (Infero-Temporal) [37] and PFC (PreFrontal Cortex) [26].

2.1.3 Maps

There is evidence that cortical columns are arranged in a smooth, locally continuous way, relative to their preferred stimuli.

The most striking examples of such organization came from the study of the Primary Visual Cortex V1 and Somatosensory / Motor Cortices. V1 maps have been studied extensively ([8] for a review, along with the original contributions by Hubel and Wiesel), and are organized in a retinotopic way, with a superposition of maps representing the same modality, such as ocular dominance, orientation (see Fig. 2.3), direction of motion and so on. Orientation maps, like the Tree Shrew's in Fig. 2.3 [5], are characterized by a very peculiar structure, with singularities (Pinwheels) around which all orientations are found.

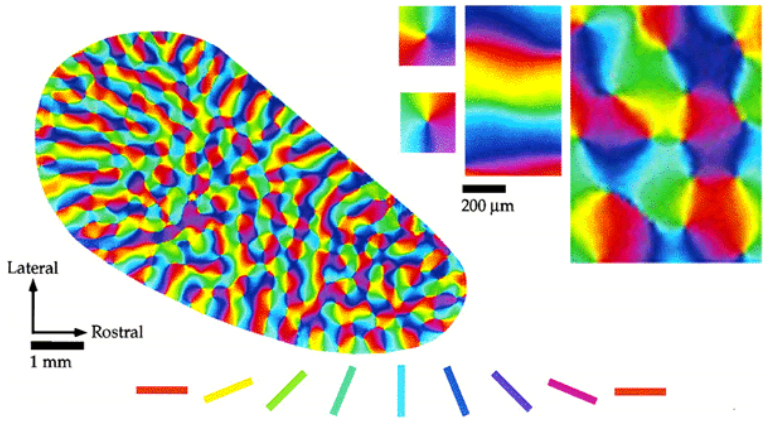

Figure 2.3: *Orientation map in Tree Shrew V1. Colors encode the minicolumns' preferred orientation [5].*

The Somatosensory Cortex, too, features a topographic representation of the whole body, with cortical magnification (ie, more cortical surface is devoted to the

representation of some parts of the body, like hands and face, than it would in relation to their real proportions). The so-called sensory and motor Homunculi are shown in Fig. 2.4.

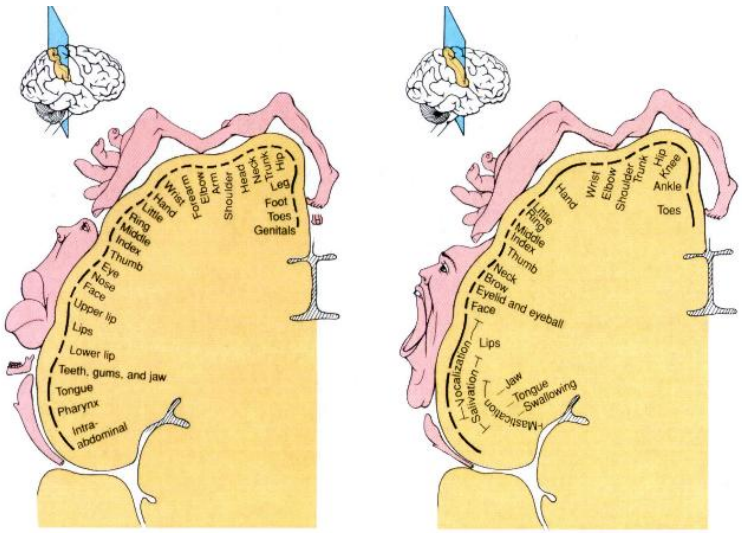

Figure 2.4: *Sensory (left) and Motor (right) homunculi.*

Different models have been proposed to explain the observed structures, with the most biological being the effect of recurrent dynamics of lateral connections [22]. Alternative works try to explain the phenomenon by moiré interference of almost regularly spaced ON- and OFF-center Retinal Ganglion Cells [29] (in relation to visual maps) or by means of a geometric interpretation [30]. Another interesting approach was undertaken by Rojer and Schwartz [32] [34], who observed that simply smoothing a random pattern of orientations (represented as unit amplitude complex numbers) leads to the appearance of orientation maps organized in close resemblance to the biological counterparts, and justified the finding as a topological result (non-retraction of $\mathbb{R}^2 \rightarrow \mathbb{S}^1$). The result holds for a map or randomly arranged Gabor filters (ie, a cortical lattice where each unit's receptive field is a randomly oriented Gabor filter), as well.

2.1.4 Visual System

The Visual System handles the processing of visual information in the Central Nervous System, and is composed by a number of complex components.

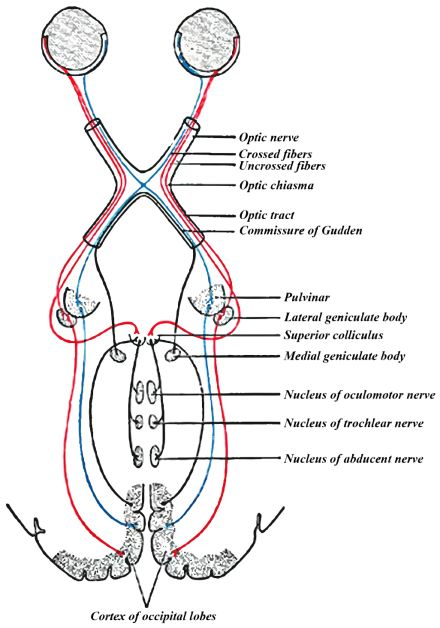

Figure 2.5: *Schematics of the first structures involved in visual processing.*

Visual processing begins in the retina, where images are filtered and encoded, and then continues in the LGN (Lateral Geniculate Nucleus) of the Thalamus, which receives information through the Optic Nerve, a one million axons bundle. Filtering in the retina is complex and has been broadly investigated; one of the most important findings was the discovery of ON- and OFF-cells, which are active respectively when a bright point in present inside and around the center of the cells' receptive fields. A detailed description of the retina is not required for the scope of this work, so we suggest more appropriate resources for more information [19]. Output fron the LGN is then relayed to the Primary Visual Cortex V1, where cortical processing begins and is then split up into two streams specialized one in the processing of shape and object identity and the other in the perception of motion, actions and spatial relationships [23]. A number of subcortical nuclei is involved with specific tasks, such as visual attention and gaze control, though in this thesis we are more focused on the high level cortical stages. Specifically, we review the first cortical areas involved, that is V1 and V2. Fig. 2.6 shows the connectivity of vision-related cortical areas.

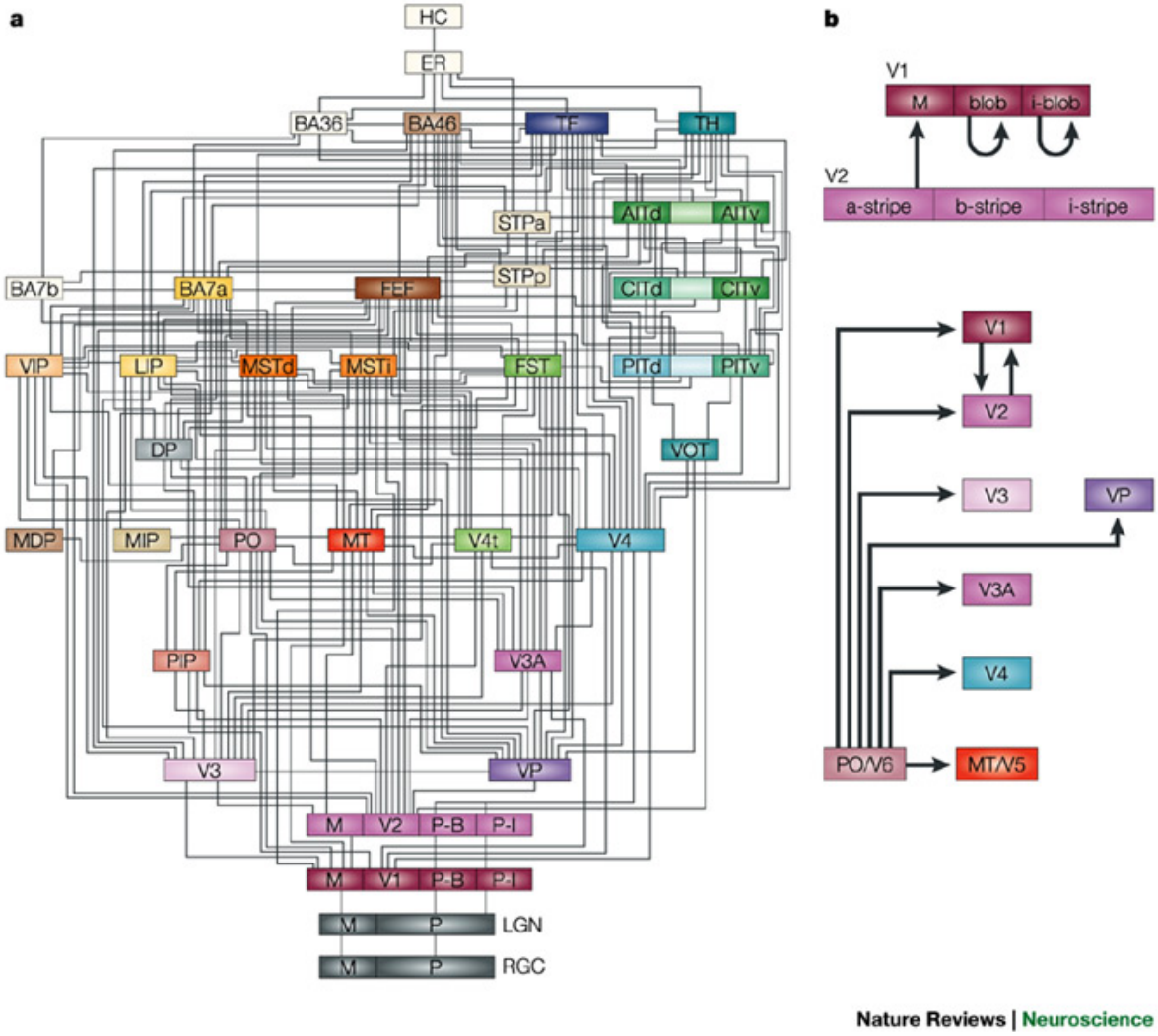

Figure 2.6: *Connectivity graph of areas in the Visual System.*

Ventral and Dorsal Pathways

The two-streams hypothesis was originally proposed by Leslie Ungerleider and Mortimer Mishkin in 1982 [23] [24] and it's now largely accepted in the scientific community. The core observation is that visual processing splits at the level of V1 / V2 to follow two different -though interconnected- paths, the *Ventral* (what) stream which goes from the Occipital to the Temporal cortex and is related to shape recognition and object identity, and the *Dorsal* (where) stream, going up to the Parietal cortex, which is involved in processing spatial relationships, actions and motion.

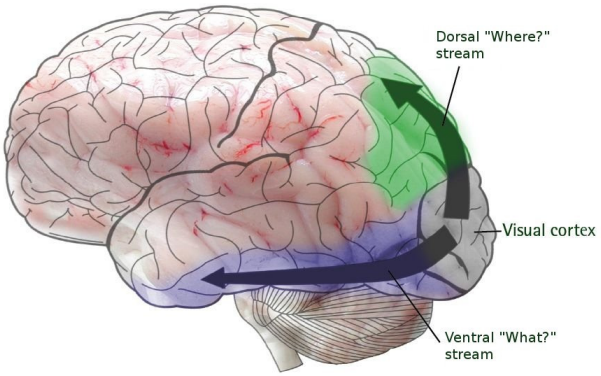

Figure 2.7: *Dorsal and Ventral pathways in visual system. Ventral stream starts from V1 to V2, V4 and up to IT and PFC*

Experimental evidence was first suggested by the study of injuries in the Inferior Temporal cortex which is linked to visual agnosia, that is the inhability to recognize objects. In contrast lesions to occipitoparietal areas led to disfunctionalities in the perception of movement, control of gaze and reaching tasks. Further studies of cell properties along both paths also provided support for this distinction, and in the past few decades, tools like PET (Positron Emission Tomography) and fMRI (functional Magnetic Resonance Imaging) opened new possibilities in the quest for a functional mapping of cortical areas, suggesting strong evidence for the theory.

V1

Primary Visual Cortex V1 is the first area in the hierarchy of the Visual System, and it's one of the most studied cortical areas. It receives feedforward input from the Thalamus (specifically from the LGN) and projects to areas V2, V3, MT (Middle Temporal), MST (Medial Superior Temporal) and FEF (Frontal Eye Fields), and provides feedback to subcortical structures such as the LGN, the thalamic retinal nucleus, the SC (Superior Colliculus), the Pulvinar Nucleus and the Pons [13]. The properties of this well studied area have been extensively investigated by Hubel and Wiesel, in a series of key contributions [16] [17] [18] and by Van Essen [9].

Functionally, V1 shows retinotopy (ie, neighboring points on the retina map to neighboring positions in the cortex) and contains a complete map of the visual field. Moreover, the retinal image is distorted so that the central part corresponding to the Fovea -the central 2% of the image- covers 50% of the cortical surface. It has been estimated that V1 is composed of around 140 million neurons per hemisphere in humans, and has an average surface of 25-30 cm^2 [20].

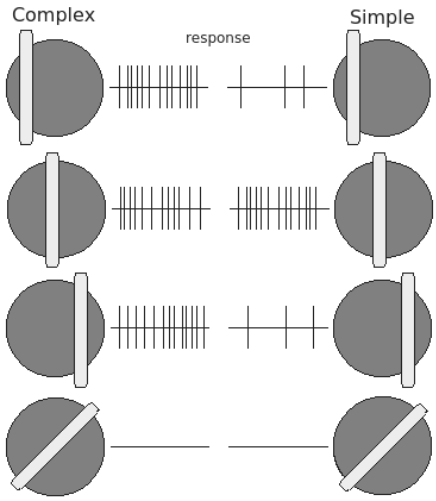

Figure 2.8: *Response of Simple and Complex cells in V1. Complex cells fire whenever their preferred stimulus is present, whereas Simple cells only fire when it is present at a definite position.*

Neurons in V1 are selective to a set of features, like oriented lines, spatial frequency, direction of motion, temporal frequency, disparity (and ocular dominance) and color (through color-opponent units). Their receptive fields are precisely localized and they are about 0.5 - 2 degrees in size near the fovea. A special mention goes to orientation selective cells, because of the extensive research and amount of data (both in terms of single-unit and map organization studies). A striking feature of these cells is their division between Simple and Complex cells, with the first being selective to specifically oriented bars at definite positions inside their receptive field, and the others producing a sustained response whenever the preferred stimulus is present, with local invariance to its position. A schematic of this difference is shown in Fig. 2.8, which plots the spiking activity of ideal Simple and Complex cells tuned to vertical bars.

2.2 Computation

The computational background is mostly based on the well estabilished Hebbian theory of synaptic plasticity. Morover, we present three models at different levels of detail, that is *Unit* (representing cortical columns) through Hebbian Learning, *Maps* with lateral interaction and *System* by taking advantage of higher level features of cortical processing, such as the building of invariant representations of external stimuli.

2.2.1 Hebbian Learning

Hebbian Learning [15], often summarized as "Cells that fire together, wire together" has been a central topic in computational neuroscience for more than half a century now. For practical applications, though, it's typically preferred to use *Oja's rule* [28], which solves all the original stability problems through multiplicative normalization. Its dynamics is described by

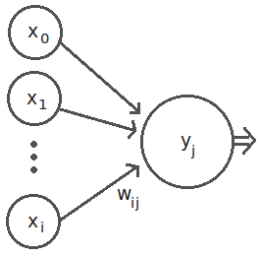

Figure 2.9: *Hebbian unit*

$$y = \sum_{\Omega} x_i w_i \tag{2.1}$$

$$\Delta w_i = \eta y(x_i - y w_i), \forall i \in \Omega \tag{2.2}$$

where y is the response of the simulated unit to input vector $\vec{x}$, and Ω is the unit's receptive field. Still, the original model as formulated in Eq. 2.2 is intended to be single unit, and can only make its weight vector $\vec{w}$ converge to the top eigenvector of the covariance matrix of the inputs (i.e. the first principal component). Many modifications have been proposed to let a network of units learn different eigenvectors, but from now on we will only consider those by T. Sanger [33] -namely, the *Generalized*

Hebbian Algorithm, GHA-, which combine Oja's rule with the Gram-Schmidt process

$$\Delta w_{ij} = \eta y_j (x_i - \sum_{k=0}^{j} y_k w_{ik}) \tag{2.3}$$

with w_{ij} repesenting the strength of the connection between the i-th afferent input and the j-th unit. It has been shown that Eq. 2.3 with p units makes the weights to converge to the first p principal components of the inputs [33]. An example of weights after convergence is shown in Fig. 2.10.

Figure 2.10: 30 *weights corresponding to the first* 30 *Principal Components of images of oriented gaussians. Weights were learnt according to Eq. 2.3 with specific simulations in the context of this thesis.*

However, we are more interested in sampling a bigger variety of the top components, rather than computing a full PCA. For instance, with reference to Fig. 2.10, we might want to make the units' weights converge to a bigger variety of orientations (like the 2^{nd} and 3^{rd} units from the left)

Another set of simulations was run by masking (i.e., multiplying) the input receptive field with a Gaussian filter, to better model the localization of the receptive fields, rather than just hard-limiting them. An example of such a simulation is shown in Fig. 2.11.

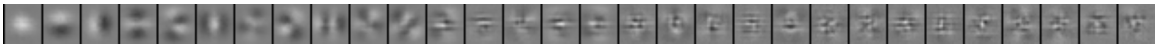

Figure 2.11: *Weights computed as in Fig. 2.10, representing the top Principal Components of uniformly translating natural images, seen through a gaussian aperture with* $\sigma = 6$.

Hebbian learning is also used to solve different problems, by setting the appropriate constraints. It has been used to perform ICA (Independent Components Analysis) [14] by implementing lateral inhibitory connections updated with the so-called *Anti-Hebbian* rule, that is

$$\Delta w_{ij} = -\eta y_i y_j \tag{2.4}$$

More generally, we always need some kind of Competition between the Hebbian units to force their weights to converge to different vectors. Common algorithms are WTA (Winner Take All), k-WTA, SotMAX or sparseness constraints, like in [38].

2.2.2 HMAX

HMAX is a biologically motivated framework, based on a quantitative theory of the organization of the ventral stream of the visual system [36] [35] [27], which addresses the problem of how visual cortex recognizes objects.

Specifically, the system models the first hundreds of milliseconds of feedforward cortical processing since the presentation of a new image, in order to avoid interference from feedback connections.

The model is based on the construction of an increasingly invariant representation of features, by alternating stages of *template matching* and *spatial pooling* across a hierarchy of processing layers. Higher stages in the hierarchy also correspond to higher features' complexity and bigger receptive fields, similar to the biological counterpart.

In its basic form, the model is made up of 4 layers, where S "Simple cells" layers (S1 and S2) alternate with C "Complex cells" layers (C1 and C2), implementing respectively the feature matching and the pooling operations, as in Figure 2.12.

Pre-processing: the image to be processed is first used to build a gaussian pyramid (eg, 10 scales, each one a factor $\sqrt[4]{2}$ smaller than the last [27])

S1: S1 layer takes the pyramid as input, and convolves every scaled image with a set of N_g Gabor filters (similar to V1 Simple Cells tuned to gabor-like stimuli),

producing another pyramid whose elements are N_g dimensional vectors. The filters are computed as

$$G(x,y) = e^{-\frac{x_0^2+\gamma^2 y_0^2}{2\sigma^2}} \cos(\frac{2\pi}{\lambda} x_0) \tag{2.5}$$

$$\begin{cases} x_0 = x\cos(\theta) + y\sin(\theta) \\ y_0 = -x\sin(\theta) + y\cos(\theta) \end{cases} \tag{2.6}$$

where γ is the aspect ratio of the filter, θ the preferred orientation, σ the effective width and λ the wavelength. Example parameters are $\theta = \{0, \frac{\pi}{4}, \frac{\pi}{2}, \frac{\pi}{4}\} \rightarrow N_g = 4$, $\gamma = 0.3$, $\sigma = 2.0$, $\lambda = 3.5$ [36]

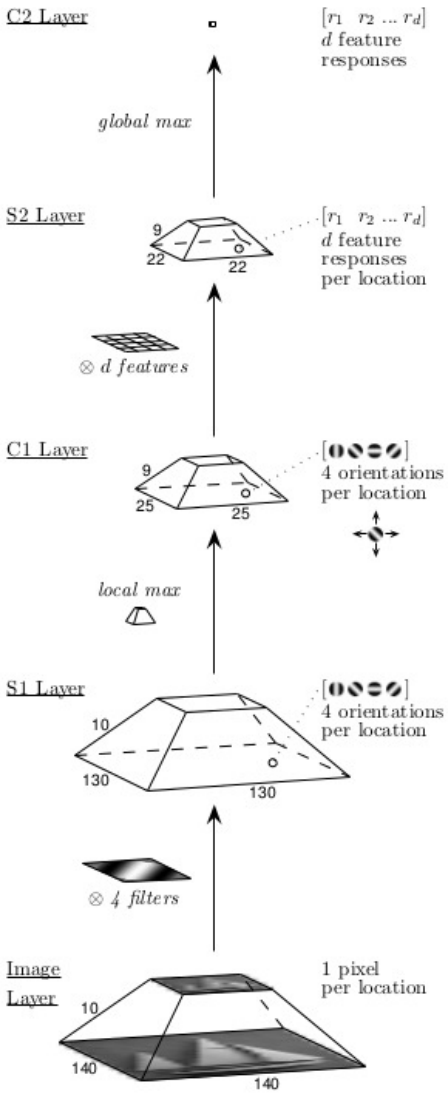

Figure 2.12: *HMAX model (from [27])*

C1: C1 layer processes the pyramid from S1 to produce a similar (smaller) one. Being a C layer, it implements a pooling operation that is, in this case, a max function over local, overlapping, neighborhoods and adjacent scales.

S2: S2 cells are modeled as RBF (Radial Basis Function) units, and produce a multidimensional pyramid whose units are N dimensional vectors, with N being the number of patches the RBFs are tuned to (usually $N \approx 1000$). Output response for any input X (C1, at every position and scale) and patch P_i is given by

$$r = e^{-\frac{\|X-P_i\|^2}{2\sigma^2\alpha}} \tag{2.7}$$

$$\alpha = \left(\frac{n}{4}\right)^2 \tag{2.8}$$

with X and P_i being n x n x N_g blocks (that is, n x n patches fora every orientation)

C2: The last layer implements a global pooling, and outputs a N-dimensional vector, whose elements are the maximum over every position and scale for each S2 patch.

Learning: Learning in the model occurs in S2 layer, and is performed by collecting a number of C1 patches at random positions, scales and sizes ($n = \{4, 8, 12, 16\}$), with a score function (eg, energy) to select the most discriminative ones. It has been tested both extracting C1 patches over all the orientations [35] and in a sparse fashion, selecting the dominant one for all the element of the patches [27].

Classification: even though the output from the model is represented by the C2 responses, higher level classification for object recognition is usually performed by training a linear classifier such as SVM (Support Vector Machine) on the output vector. For a comparison of performance in reference to other systems we suggest [35] [27].

2.2.3 LISSOM

LISSOM (Laterally Interconnected Synergetically Self-Organizing Map) is a self-organizing model of the development of feature maps in Primary Visual Cortex V1 [4] [1] [22] [2]. The model is similar to Kohonen Self Organizing Maps, but differently from them LISSOM retains a level of biological plausibility, in that it reproduces some of the most prominent neocortical behaviors. Kohonen SOMs only allow a single winner per iteration, which limits practical use to only small patches, with a strong lateral inhibition equivalent. Also, those maps lack any retinotopy and receptive fields are not localized. In contrast, LISSOM

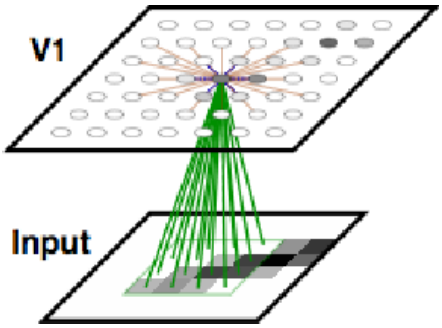

Figure 2.13: *LISSOM architecture : the modeled layer is fed an afferent input, and presents lateral connections that are short-range excitatory and long-range inhibitory*

employs recurrent lateral interactions -which are learnt at run-time- to sharpen activity around strongly activated spots (multiple *local* winners occur at the same time, instead of a global winner). Moreover, activaton is computed as a function of dot product between the afferent input, localized retinotopically, and the unit's weights (rather than computing their euclidean distance). Currently the model (GCAL, gain-control adaptive laterally connected) also features mechanisms for automatic homeostatic plasticity in place of the activation thresholds, and gain control to remove local contrast in the input [3] [39].

In practice, LISSOM is implemented as a *layer* made up of processing *units*. The layer is fed another layer as input (eg, an image, representing a "retina", or another layer [31]), and specifically, every unit has an afferent receptive field localized in the corresponding position of the input layer (ie, retinotopically). The Computation of the activation of the units requires two steps: computing the raw output, and settling activation with recurrent interaction from lateral connections. At the first step we compute the initial activation ζ_j of unit j

$$\zeta_j = \sum_{i \in Afferent\{j\}} x_i w_{ij} \tag{2.9}$$

with x being the input and w being the afferent weights linking input unit i to layer unit j. We can then compute the final activation by letting lateral connection reach an equilibrium

$$y_j(t) = \sigma \left(\zeta_j + \gamma_E \sum_{i \in exc\{j\}} w_{E_i} y_i(t-1) - \gamma_I \sum_{i \in inh\{j\}} w_{I_i} y_i(t-1) \right) \tag{2.10}$$

$$\sigma(x) = \begin{cases} 0 & x \leq \delta \\ \frac{x-\delta}{\beta-\delta} & \delta < x < \beta \\ 1 & x \geq \beta \end{cases} \tag{2.11}$$

where $y_j(t)$ is the output of unit j at step t (recurrent iterations are simulated for T times, eg $T = 10$), w_{E_i} and w_{I_i} are the strenghts of the lateral connections. $\sigma(x)$ is a piece-wise approximation of the sigmoidal function, and it models threshold / saturation phenomena.

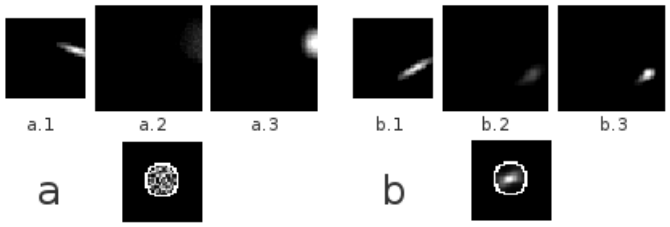

Figure 2.14: *Group* ***a*** *shows an example input fed into the network (**a.1**), the raw output before settling (**a.2**) and the final output after a number of recurrent interations of lateral excitation and inhibition (**a.3**). Group* ***b*** *represents the same data, after* 10000 *training iterations: we can see that the response is sharp and it's localized into an activity bubble. Bottom row shows one of the afferent receptive field's weights (untrained vs trained). This figure was generated with Topographica software [2].*

Once activation has settled, all the weights are updated according to classical Hebbian rule, and weights are normalized to unit sum (separately for afferent, excitatory and inhibitory).

$$w_{ij}(t+1) = \frac{w_{ij}(t) + \eta x_i y_j}{\sum_k w_{kj}(t) + \eta x_k y_j} \tag{2.12}$$

η is the learning rate, and x_i represents y_i when updating lateral weights.

It has been shown experimentally that LISSOM layers are capable of modeling the development of many feature maps found in V1. This can be seen in figure 2.15, which also shows an example output produced from an input image, where we can identify many different activity bubbles, whose units encode information about the edges in their receptive fields, according to their preferred orientations.

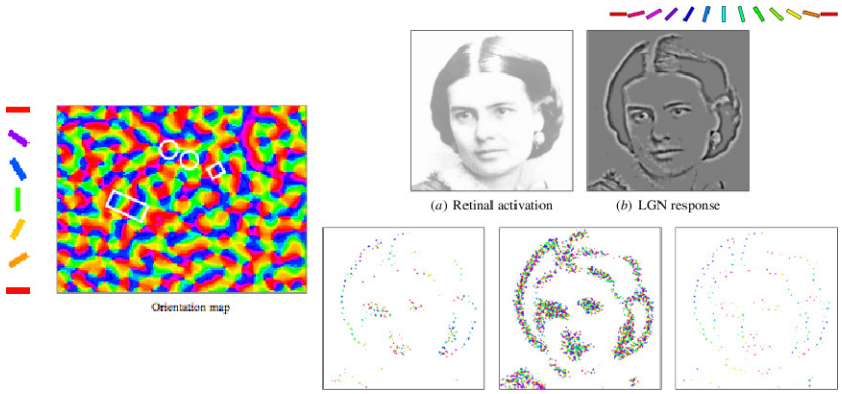

Figure 2.15: *Left is a trained LISSOM layer whose units have been color-coded to represent their preferred orientation. Right is the output of the trained layer when presented the retinal image (a). (b) shows the LGN-filtered image, which is fed into the layer, while the bottom row contains three different outputs of the layer, under different gain-contrast settings (color coded for the units' preferred orientations). Like Fig. 2.14, this figure was generated with Topographica software [2].*

CHAPTER 3

Cortical Learning

Now that we have reviewed the background of this research we can outline the core topic. The problem we face is part of the broader task of developing a computational model of the Neocortex, and is motivated by the relative lack of fast algorithms to simulate the development of cortical receptive fields. Morover, we want to develop a model inspired by the biological system, but targeted for applications, for instance in humanoid robotics and computer vision.

Now, the first property we want the system to have is full unsupervised learning of the units' weights, possibly with a stable output representation computed using them, and given as a 2D activity map. Also, we would expect the final receptive fields to be sparse and in close resemblance to those identified in V1, ie, Gabor filters.

3.1 Methods

We choose to model a 2D patch of a neural layer, whose units represent overall activity of cortical minicolumns. Every unit is associated with an afferent weight matrix to model its receptive field, and a specific position in the input map (correspondent to its position in the layer). Minicolumns are grouped into non-overlapping square clusters to approximante the local dynamics of macrocolumns. We decided to model the Primary Visual Cortex, so the input is passed through a very basic model of processing in the Retina+LGN. A picture of the system is shown in Fig. 3.1. Also, computational complexity was considered, in that we wanted it not to be greater than

$O(N^2)$, with N being the width / height of the map.

We implemented our simulations in C++ (code in Appendix A).

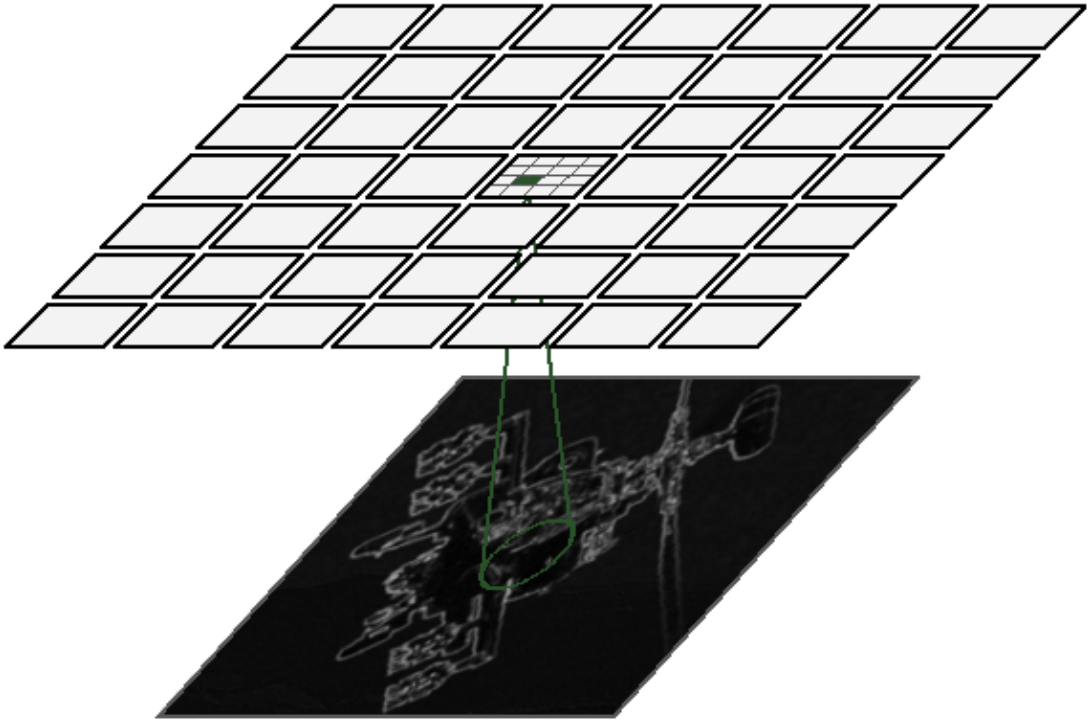

Figure 3.1: *Schematics of the system. The model layer is subdivided into a matrix of units, which have partially overlapping receptive fields (one is shown in green for reference) and are grouped into blocks.*

3.1.1 Input

The input presented to the model layer is an image patch, whose pixels represent the activity of a very simplified model of LGN neurons. In our experiments, we used images from the Caltech101 database [12] as inputs to the Retina+LGN simulator.

At each iteration, the system samples an image uniformly at random, converts it to grayscale and rotates it by a random angle. Then we approximate the effect of ON- and OFF-center cells (we computed a single output per position in the retina, employing negative values, though similar results can be achieved separating the

positive and negative responses in two maps, which are both used as input to the cortical layer) by convolving the image with a DoG (Difference of Gaussians) filter

$$DoG(x,y) = \frac{1}{2\pi\sigma_1^2} e^{-\frac{x^2+y^2}{2\sigma_1^2}} - \frac{1}{2\pi\sigma_2^2} e^{-\frac{x^2+y^2}{2\sigma_2^2}} \tag{3.1}$$

where we used $\sigma_1 = 0.875$ and $\sigma_2 = 1.4$, with filters of size $N_{DoG} = 7$. Then a fixed size square is extracted from the output at a random position while the image is translated for a number of iterations (in the experiments we used numTranslationSteps= 15, translationSpeed= 5 $pixels/step$), and at each step the final output was set to the difference of consecutive frames to simulate a temporal derivative operator. The size of the cropped region is set to be the same as we need the layer's input size to be (in our experiments it was set to $inputN = N + RF_{size} - 1$, where N is the size of the model layer and RF_{size} the width of the recepive field). A diagram showing the output after each processing operation is shown in Fig. 3.2.

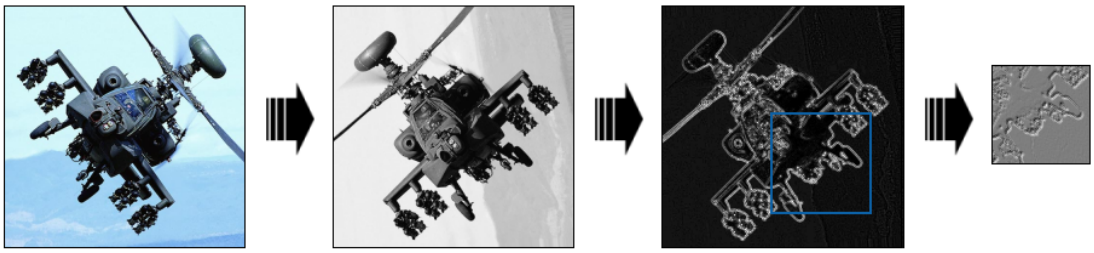

Figure 3.2: *Example of processing: images (a) are converted to grayscale and rotated at random (b), then they are convolved with a DoG filter (c) and the output is finally computed by translating the image (in (c)) in a random direction, computing the difference between consecutive frames and cropping a region.*

3.1.2 Activation

In the model, every unit j in the map is associated to a weight vector $\vec{w}_j$. Activation for each unit is computed as a function of the normalized dot product between its

weight and the portion of the input which falls under its receptive field $\vec{x}$.

$$\tilde{y}_j = \frac{\vec{w}_j \cdot \vec{x}}{\|\vec{w}_j\|\|\vec{x}\|} \tag{3.2}$$

$$y_j = f(\tilde{y}_j) \tag{3.3}$$

where y_j is the output of layer unit j, and f is a function which can be used to introduce non-linearities in the activation. In the experiments we show in this thesis, we always used the identity function $f(x) = x$. Also, in some tests, we forced the receptive field to be in a Gaussian envelope, which seems a more natural way to localize the RFs than just truncating the input outside the units' preferred positions in the retina. In practice, we multiplied the input vector with a Gaussian mask

$$x_i = G(i)\tilde{x}_i \tag{3.4}$$

where $G(i)$ is the Gaussian mask centered on the unit's receptive field with a fixed σ_x.

3.1.3 Learning

The main part of the model is the learning algorithm, which controls how the units' weights are updated at each iteration. The rule is based on Competitive Learning, mediated by a hard WTA (Winner Take All) local to each macrocolumn, and extends the Oja's Rule [28] [21].

Specifically, we first compute the maximum activation for each macrocolumn M_k

$$\mathrm{Z}_k = \max_{j \in M_k} y_j \tag{3.5}$$

then, we update the weights of all the units in the macrocolumn according to

$$\Delta w_{ij} = \eta y_j (x_i - y_j w_{ij}) \tag{3.6}$$

where $\eta = \eta_0$ (in our experiments $\eta_0 = 0.007$) for $y_j = Z_k$, and $\eta = -\eta_0/100 \; \forall y_j < Z_k$. Learning rate η_0 is fixed during all the simulation.

3.2 Results

We run our simulations for 100.000 iterations (though good convergence was reached after the first tens of thousands) over a range of parameters. All the plots presented in this section were either computed as 2x2 or 6x6 matrices of macrocolumns (for plotting purpose only), each one composed by 4x4 units, and receptive field size was set to $RF_{size} = 13$, unless otherwise stated. The pictures show the learnt weights of each unit, grouped per block, and converted to gray scale images, where light gray represents zero and brigher/darker shades stand for positive and negative values, respectively.

- Learning of weights with basic settings (Fig. 3.3)

  The first set of simulations were tested in relation to the change of different parameters, such as learning rate and size of modules and receptive fields. Inputs were patches processed like described in Section 3.1.1.

- A smaller map developed like first, but showing the units' weights in greater detail (Fig. 3.4)

  For ease of presentation we also trained a small layer, to show the weights after development with better clarity. Fig. 3.4 highlights the fine, smooth details of the orientation tuning.

- Weights were trained on inputs masked with a Gaussian filter (Fig. 3.5)

  Another set of simulations was run by multiplying the units' receptive fields with a Gaussian mask, to provide a smoother localization function. Most of the weights after convergence closely remind of Gabor filters.

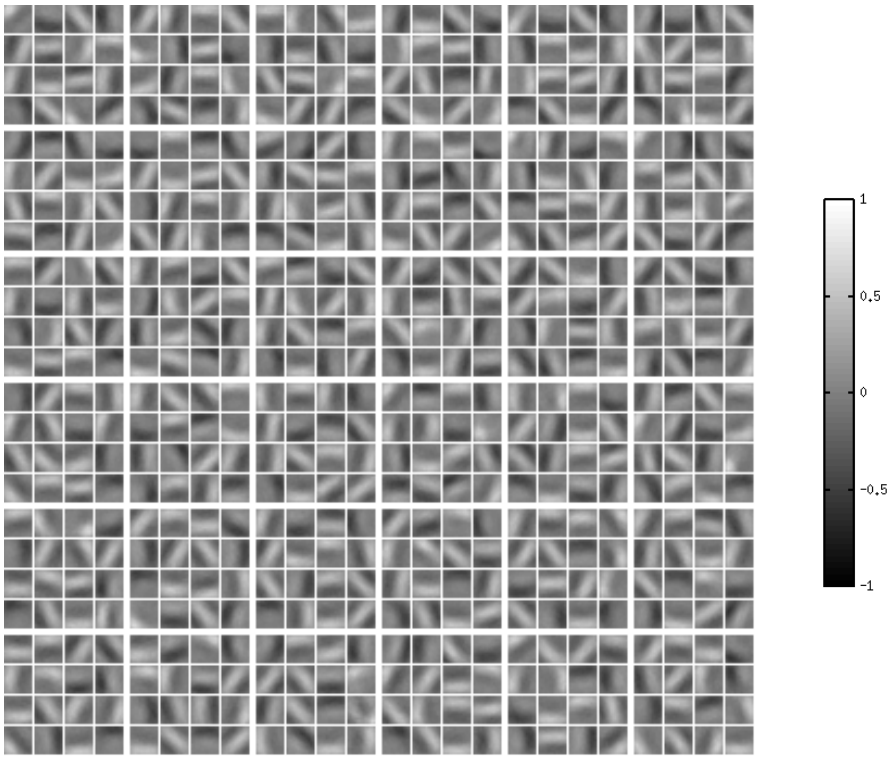

Figure 3.3: *Converged weights of 6x6 modules (macrocolumns), each composed by 4x4 units (minicolumns) with no gaussian aperture.* $RF_{size} = 13$*, that is the filters are* $13x13$ *in size.*

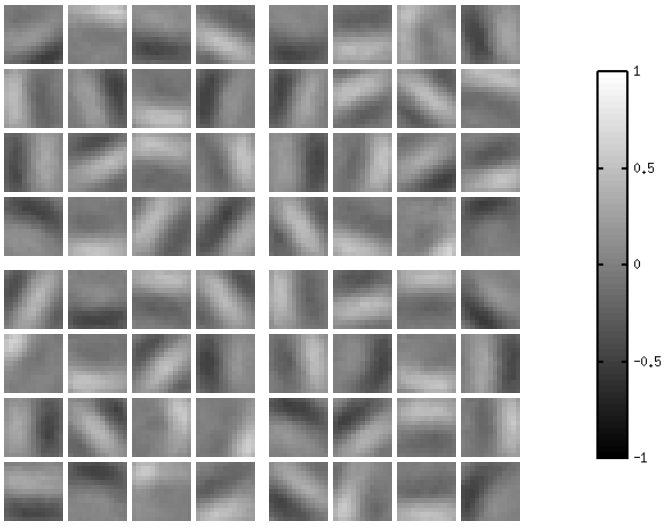

Figure 3.4: *Like Fig. 3.3 with 2x2 macrocolumns.*

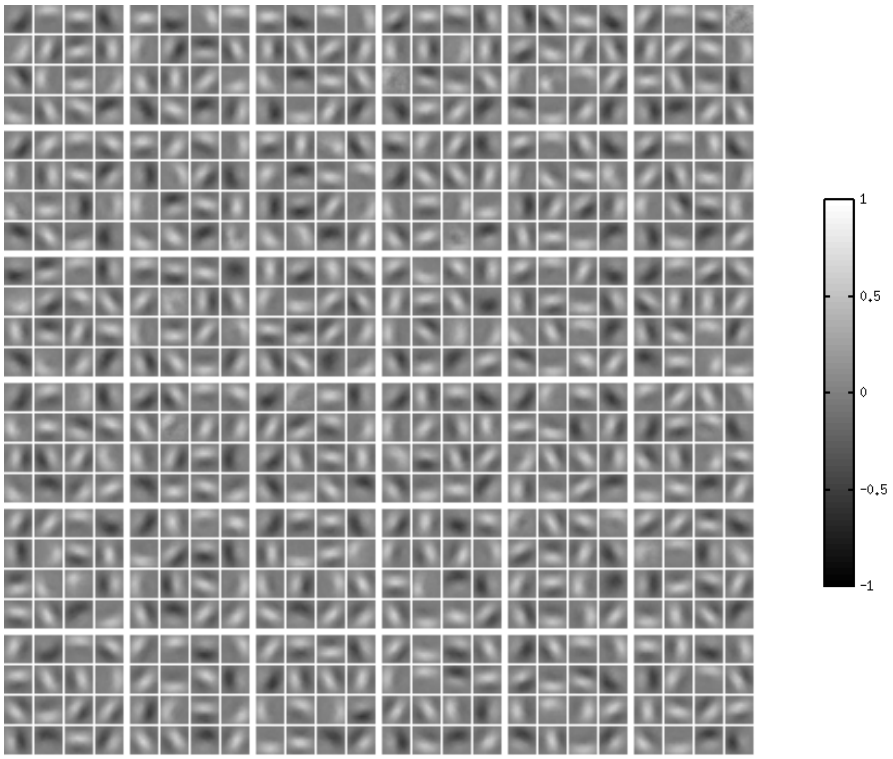

Figure 3.5: *Like Fig. 3.3 but with inputs multiplied by a gaussian filter with* $\sigma = 6$.

As we can see, weights after convergence show a preference for specifically oriented lines, which is compatible with other models of V1 and with experimental physiological evidence. To further explore this result, we fitted the weights in Fig. 3.4 with 2D Gabor filters (Eq. 2.5), computing the parameters which made them most similar. For ease of computation, we manually set most of the values, which were constant for all the weights, and we optimized for orientation θ and position (x_0, y_0). Fig. 3.6 shows an example of such reconstruction, along with the Gabor parameters used to generate the filters. A broader view is shown in Fig. 3.7, featuring the full matrix of reconstructed weights.

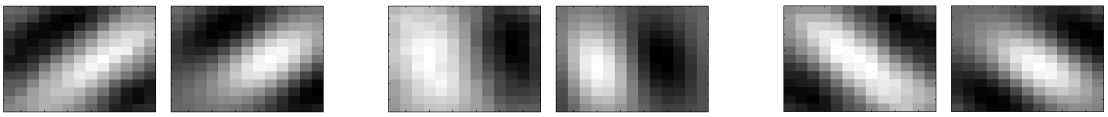

(a) **(b)** **(c)**

Figure 3.6: *Comparison between learnt weights (left image in every subplot) and corresponding 2D Gabor filters reconstructed (right image). For every filter,* $\psi = 0$, $\lambda = 4\pi$, $\gamma = 1.5$, $\sigma = 6$ *(filter size set to* $13x13$*), and* $\theta_1 = 45°$ *(3.6a),* $\theta_2 = 100°$ *(3.6b),* $\theta_3 = 135°$ *(3.6c).*

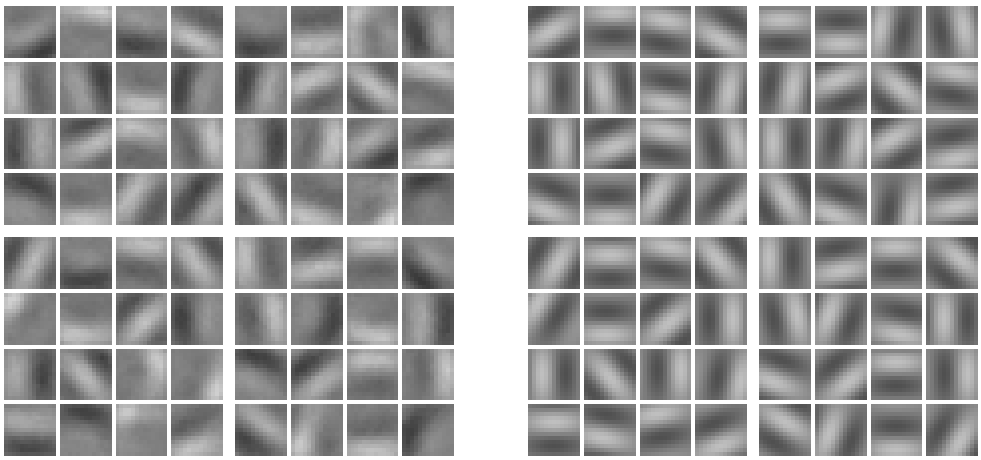

(a) **(b)**

Figure 3.7: *Full array of weights from Fig. 3.4 are shown in (3.7a) by side with the reconstructed Gabor filters (3.7b). Parameters are the same as Fig. 3.6 except for* $\sigma = 8$.

CHAPTER 4

DISCUSSION AND CONCLUSIONS

As we can see from the plots in section 3.2 all the units but a little number develop orientation selectivity by looking at translating images, and they show interesting features changing the main parameters.

Future work will be focused primarily on the use of Competitive Learning algorithms like ours in learning multi-stage cortical weights in hierarchies, with special interest in the mechanisms underlying the increase in invariance and, in this context, the development of the receptive fields of Complex Cells. We are also going to validate our system using inputs from different modalities or with bigger dimensionality incorporating, for instance, binocularity and color representation, speaking about the visual system. Last but not least, we will research the relation between our learning algorithm and the formation of cortical maps, with the possible introduction of some kind of local correlation, which would model the dynamics of short-range excitatory synapses between minicolumns.

In conclusion, results look promising, and they suggest that the most basic properties of cortical response could be modeled with computationally friendly operations, such as the Winner Take All. In this regard, the system we presented could be used in computer vision applications and possibly in other machine learning applications, as well.

BIBLIOGRAPHY

[1] Jan Antolik and James A Bednar. Development of maps of simple and complex cells in the primary visual cortex. *Frontiers in Computational Neuroscience*, 5(17), 2011.

[2] James A Bednar. Topographica: building and analyzing map-level simulations from python, c/c++, matlab, nest, or neuron components. *Frontiers in Neuroinformatics*, 3(8), 2009.

[3] James A. Bednar. Building a mechanistic model of the development and function of the primary visual cortex. *Journal of Physiology-Paris*, (0), 2012.

[4] James A. Bednar and Risto Miikkulainen. Tilt aftereffects in a self-organizing model of the primary visual cortex. *Neural Computation*, 12:1721–1740, 2000.

[5] William H. Bosking, Ying Zhang, Brett Schofield, and David Fitzpatrick. Orientation selectivity and the arrangement of horizontal connections in tree shrew striate cortex. *The Journal of Neuroscience*, 17(6):2112–2127, 1997.

[6] Gary Bradski. The OpenCV Library. *Dr. Dobb's Journal of Software Tools*, 2000.

[7] Manuel F. Casanova. *Neocortical Modularity and the Cell Minicolumn*. 2005.

[8] Bruce M. Dow. Orientation and color columns in monkey visual cortex. *Cerebral Cortex*, 12(10):1005–1015, 2002.

[9] David C. Van Essen and Charles H. Anderson. Information processing strategies and pathways in the primate visual system. *An Introduction to Neural and Electronic Networks*, pages 45–76, 1995.

[10] Oleg Favorov and Barry L. Whitsel. Spatial organization of the peripheral input to area 1 cell columns. i. the detection of 'segregates'. *Brain Research Reviews*, 13(1):25 – 42, 1988.

[11] Oleg V. Favorov and Mathew E. Diamond. Demonstration of discrete place-defined columnssegregatesin the cat si. *The Journal of Comparative Neurology*, 298(1):97–112, 1990.

[12] Li Fei-Fei, Rob Fergus, and Pietro Perona. Learning generative visual models from few training examples: An incremental bayesian approach tested on 101 object categories. 2004.

[13] Daniel J. Felleman and David C. Van Essen. Distributed hierarchical processing in the primate cerebral cortex. *Cerebral Cortex*, 1(1):1–47, 1991.

[14] Peter Földiák. Forming sparse representations by local anti-hebbian learning. *Biological Cybernetics*, 64:165–170, 1990.

[15] Donald O. Hebb. *The organization of behavior*. 1949.

[16] D. H. Hubel and T. N. Wiesel. Receptive fields, binocular interaction and functional architecture in the cat's visual cortex. *The Journal of Physiology*, 160(1):106–154, 1962.

[17] D. H. Hubel and T. N. Wiesel. Receptive fields and functional architecture of monkey striate cortex. *The Journal of Physiology*, 195(1):215–243, 1968.

[18] David H. Hubel and Torsten N. Wiesel. Sequence regularity and geometry of orientation columns in monkey striate cortex. *Journal of Comparative Neurology*, 158(3):267–294, 1974.

[19] Eric R. Kandel, James H. Schwartz, and Thomas M. Jessell. *Principles of Neural Science*. 2000.

[20] G. Leuba and R. Kraftsik. Changes in volume, surface estimate, three-dimensional shape and total number of neurons of the human primary visual cortex from midgestation until old age. *Anatomy and Embryology*, 190:351 – 366, 1994.

[21] Timothee Masquelier, Thomas Serre, Simon Thorpe, and Tomaso Poggio. Learning complex cell invariance from natural videos: A plausibility proof. Technical report, MIT, CSAIL, CBCL, 12 2007.

[22] Risto Miikkulainen, James A. Bednar, Yoonsuck Choe, and Joseph Sirosh. *Computational Maps in the Visual Cortex*. Springer, 2005.

[23] Mortimer Mishkin and Leslie G. Ungerleider. Contribution of striate inputs to the visuospatial functions of parieto-preoccipital cortex in monkeys. *Behavioural Brain Research*, 6(1):57 – 77, 1982.

[24] Mortimer Mishkin, Leslie G. Ungerleider, and Kathleen A. Macko. Object vision and spatial vision: two cortical pathways. *Trends in Neurosciences*, 6(0):414 – 417, 1983.

[25] Vernon B. Mountcastle. Modality and topographic properties of single neurons of cat's somatic sensory cortex. *Journal of Neurophysiology*, 20(4):408–434, 1957.

[26] Vernon B. Mountcastle. The columnar organization of the neocortex. *Brain*, 120(4):701–722, 1997.

[27] Jim Mutch and David G. Lowe. Object class recognition and localization using sparse features with limited receptive fields. *International Journal of Computer Vision (IJCV)*, 80(1):45–57, October 2008.

[28] Erkki Oja. Simplified neuron model as a principal component analyzer. *Journal of Mathematical Biology*, 15(3), 1982.

[29] Se-Bum Paik and Dario L. Ringach. Retinal origin of orientation maps in visual cortex. *Nat Neurosci*, 14(7):919–925, Jul 2011.

[30] Jean Petitot. The neurogeometry of pinwheels as a sub-riemannian contact structure. *Journal of Physiology-Paris*, 97(23):265 – 309, 2003.

[31] Alessio Plebe and Rosaria Grazia Domenella. Early development of visual recognition. *Biosystems*, 86(13):63 – 74, 2006.

[32] Alan S. Rojer and Eric L. Schwartz. Cat and monkey cortical columnar patterns modeled by bandpass filtered 2d white noise. *Biological Cybernetics*, 62(5), 1990.

[33] Terence D. Sanger. Optimal unsupervised learning in a single-layer linear feedforward neural network. *Neural Networks*, 2(6), 1989.

[34] Eric L. Schwartz and Alan S. Rojer. Cortical hypercolumns and the topology of random orientation maps. *Pattern Recognition*, 1994.

[35] Thomas Serre, Lior Wolf, Stan Bileschi, Maximilian Riesenhuber, and Tomaso Poggio. Robust object recognition with cortex-like mechanisms. *Pattern Analysis and Machine Intelligence, IEEE Transactions on*, 29(3):411 –426, march 2007.

[36] Thomas Serre, Lior Wolf, and Tomaso Poggio. Object recognition with features inspired by visual cortex. 2:994 – 1000 vol. 2, june 2005.

[37] Kazushige Tsunoda, Yukako Yamane, Makoto Nishizaki, and Manabu Tanifuji. Complex objects are represented in macaque inferotemporal cortex by the combination of feature columns. *Nature Neuroscience*, 4(8):832–838, August 2001.

[38] Ray H. White. Competitive hebbian learning: Algorithm and demonstrations. *Neural Networks*, 5(2):261–275, February 1992.

[39] Stuart P. Wilson, Judith S. Law, Ben Mitchinson, Tony J. Prescott, and James A. Bednar. Modeling the emergence of whisker direction maps in rat barrel cortex. *PLoS ONE*, 5(1):e8778, 01 2010.

APPENDIX A

Simulations

Following is the code used to run the simulations described in Chapter 3. The algorithms described are implemented by the *Retina* and the *Layer* classes:

- *Retina* takes care of processing input images as described in 3.1.1
- *Layer* provides support for management of data structures required by the model, and implements the learning algorithm in 3.1.3 (as well as computing output activation as in 3.1.2)

The software requires linking with the OpenCV computer vision library [6].

```
#include <stdio.h>
#include <stdlib.h>
#include <time.h>
#include <math.h>
#include <vector>
#include <algorithm>

#include <cv.h>
#include <highgui.h>

#include <iostream>
using namespace std;

#define RETINA_MODE_DEBUG 0
#define RETINA_MODE_VIDEO 1
```

```
#define RETINA_MODE_CALTECH 2

#define writeint(a_, fp_) fwrite(&a_, sizeof(int), 1, fp_);
#define writefloat(a_, fp_) fwrite(&a_, sizeof(float), 1, fp_);

#define readint(a_, fp_) fread(&a_, sizeof(int), 1, fp_);
#define readfloat(a_, fp_) fread(&a_, sizeof(float), 1, fp_);

// First Stage of processing
class Retina {
public:
  int width, height;

  int videoW, videoH;
  CvCapture *capture;
  IplImage *prev, *cur, *tmp, *g1, *g2;
  IplImage *image;

  int mode;

  int caltech_r, caltech_x, caltech_y, caltech_iii;
  float caltech_theta, rotate_theta;


  Retina(int w, int h, int mode_=RETINA_MODE_VIDEO);
  ~Retina();

  void getImage();

};
```

```
// Second stage of processing
class Layer {
public:
  int width, height;
  Retina *retina;

  int rf, rf21, rf2;
  float sigmaRf, sigmaRf2;
  float *gaussianAperture;
  int moduleN, numModulesW, numModulesH;

  float **weights;
  float *out;
  float *out_exp;


  Layer(int w, int h, int rf, int moduleN_, float sigmaRf_, Retina *r);
  ~Layer();

  void save(const char *file);
  Layer(const char *file, Retina *r);

  void train(int numIterations);
  void getAllWeights(IplImage *weights_out, float amp=1.0f);

};



Retina::Retina(int w, int h, int mode_) {
  this->width = w;
  this->height = h;
```

```
    this->mode = mode_;

81

    if(mode_==RETINA_MODE_VIDEO) {
      this->capture = cvCreateFileCapture("../ShowVideo.avi");
      IplImage *frame=NULL;
      while(!frame)
        frame=cvQueryFrame(capture);

      this->videoW = frame->width;
      this->videoH = frame->height;

91    this->prev = cvCreateImage(cvSize(frame->width, frame->height),
          IPL_DEPTH_8U, 1);
      this->cur = cvCreateImage(cvSize(frame->width, frame->height),
          IPL_DEPTH_8U, 1);
      cvZero(this->cur);

      this->tmp = cvCreateImage(cvSize(frame->width, frame->height),
          IPL_DEPTH_8U, 1);
      this->g1 = cvCreateImage(cvSize(frame->width, frame->height),
          IPL_DEPTH_8U, 1);
      this->g2 = cvCreateImage(cvSize(frame->width, frame->height),
          IPL_DEPTH_8U, 1);

      this->caltech_iii=0;

101   } else if(mode_==RETINA_MODE_CALTECH) {
      this->tmp = cvCreateImage(cvSize(w,h), IPL_DEPTH_8U, 1);
      this->g1 = cvCreateImage(cvSize(w,h), IPL_DEPTH_8U, 1);
      this->g2 = cvCreateImage(cvSize(w,h), IPL_DEPTH_8U, 1);

      this->caltech_iii=0;
```

```
    }

    this->image = cvCreateImage(cvSize(w, h), IPL_DEPTH_32F, 1);

}


Retina::~Retina() {
    cvReleaseCapture(&capture);

    cvReleaseImage(&prev);
    cvReleaseImage(&cur);
    cvReleaseImage(&tmp);
    cvReleaseImage(&g1);
    cvReleaseImage(&g2);

}


// Utility function: draws a randomly oriented elongated gaussian into "
    im" image
void RandomGaussian( IplImage *im, int centered=0, float thr=0.369f ) {
    const int border=4;

    const float a2=56.25;
    const float b2=2.25;

    int xc=(int)((float)rand()/(float(RAND_MAX)+1.0)*(float)(im->width-2*
        border))+border;
    int yc=(int)((float)rand()/(float(RAND_MAX)+1.0)*(float)(im->height-2*
        border))+border;
```

```
    int theta_=(int)((float)rand()/(float(RAND_MAX)+1.0)*180.0);
    theta_=theta_/15;
    theta_=theta_*15;
    float theta=(float)theta_/180.0 * 3.141592;

141

    float cost=cos(theta);
    float sint=sin(theta);

    if(centered==1) {
      xc=im->width/2;
      yc=im->height/2;
    }



151   float *imf=(float*)im->imageData;
    int p=im->widthStep/sizeof(float);
    for(int x=0; x<im->width; x++) for(int y=0; y<im->height; y++) {
      int j=x-xc;
      int k=y-yc;

      float res=exp( -(j*cost - k*sint)*(j*cost - k*sint)/a2 -(j*sint + k*
          cost)*
  (j*sint + k*cost)/b2 );

      if(res>=thr) imf[y*p+x]=res;
161   else imf[y*p+x]=0.0;
    }

  }
```

```
// Main function for "Retina" objects: generate and process input images
void Retina::getImage() {
  const float SIGMA_OUT = 1.4f;
  const float SIGMA_IN = 0.875f;

  if(mode==RETINA_MODE_DEBUG) {
    // Generate oriented gaussians
    RandomGaussian( image, 0); //centered


  } else if(mode==RETINA_MODE_CALTECH) {
    // Process Caltech101 image
    int sz = image->width;
    int maxTransl=15;

    if((caltech_iii%maxTransl)==0)
      caltech_r = (int)( (float)rand()/((float)RAND_MAX+1.0f)*9196.0f   )
          ;

    char str[80]; sprintf(str, "../Caltech101/%d.png", caltech_r);

    IplImage *tmp_ = cvLoadImage(str);
    if(!tmp_)
      cout<<str<<endl;


    IplImage *tmp = cvCreateImage(cvSize(tmp_->width, tmp_->height),
       IPL_DEPTH_8U, 1);
    cvConvertImage(tmp_, tmp);


    int mult=5;
```

```
    if((caltech_iii%maxTransl)==0) {
      caltech_x = (int)( (float)rand()/((float)RAND_MAX+1.0f)*(tmp->
          width-sz-2-2*mult*maxTransl) )+1+mult*maxTransl;
      caltech_y = (int)( (float)rand()/((float)RAND_MAX+1.0f)*(tmp->
          height-sz-2-2*mult*maxTransl) )+1+mult*maxTransl;

      int theta_=(int)((float)rand()/(float(RAND_MAX)+1.0)*360.0);
      theta_=theta_/15;
      theta_=theta_*15;
      caltech_theta=(float)theta_/180.0 * 3.141592;
//theta=1.54f;

      theta_=(int)((float)rand()/(float(RAND_MAX)+1.0)*360.0);
      theta_=theta_/15;
      theta_=theta_*15;
      rotate_theta=(float)theta_/180.0 * 3.141592;

    }


    IplImage *tmp2 = cvCreateImage(cvSize(tmp_->width, tmp_->height),
        IPL_DEPTH_8U, 1);

    float angle = rotate_theta; //caltech_theta;

    float m[6];
    CvMat M = cvMat(2, 3, CV_32F, m);

    m[0] = (float)cos(angle-3.141592f/2.0f);
    m[1] = (float)sin(angle-3.141592f/2.0f);
    m[3] = -m[1];
    m[4] = m[0];
```

```
m[2] = tmp_->width*0.5f;
m[5] = tmp_->height*0.5f;

cvGetQuadrangleSubPix( tmp, tmp2, &M );


IplImage *g1=cvCreateImage(cvSize(tmp_->width, tmp_->height),
    IPL_DEPTH_8U, 1);
IplImage *g2=cvCreateImage(cvSize(tmp_->width, tmp_->height),
    IPL_DEPTH_8U, 1);
cvSmooth(tmp2, g1, CV_GAUSSIAN, 7, 0, SIGMA_OUT);
cvSmooth(tmp2, g2, CV_GAUSSIAN, 7, 0, SIGMA_IN);
cvAbsDiff(g1, g2, tmp);
cvReleaseImage(&g1);
cvReleaseImage(&g2);

cvConvertScale(tmp, tmp, 10);


float *imf = (float*)image->imageData;
int p = image->widthStep/sizeof(float);

int translX = (caltech_iii%maxTransl)*mult*cos(caltech_theta);
int translY = (caltech_iii%maxTransl)*mult*sin(caltech_theta);
int translXold = (caltech_iii%maxTransl-1)*mult*cos(caltech_theta);
int translYold = (caltech_iii%maxTransl-1)*mult*sin(caltech_theta);
for(int i=0; i<sz; i++) {
  for(int j=0; j<sz; j++) {
    float a = (float)( ((unsigned char*)tmp->imageData)[ (caltech_y+
        j+translY)*tmp->widthStep + (caltech_x+i+translX) ] - ((
        unsigned char*)tmp->imageData)[ (caltech_y+j+translYold)*tmp
        ->widthStep + (caltech_x+i+translXold) ] )/255.0f;
```

```
        imf[ (j)*p + (i) ] = a;

      }
    }

    cvReleaseImage(&tmp_);
    cvReleaseImage(&tmp);
    cvReleaseImage(&tmp2);


    caltech_iii++;

  } else if(mode==RETINA_MODE_VIDEO) {
    // Process image from video

    IplImage *frame = NULL;
    frame = cvQueryFrame(capture);

    if(!frame) {
      cvReleaseCapture(&capture);
      capture = cvCreateFileCapture("../ShowVideo.avi");
      while(!frame)
        frame=cvQueryFrame(capture);

    }

    cvCopy(cur, prev);
    cvConvertImage(frame, cur);

    cvSmooth(cur, g1, CV_GAUSSIAN, 5, 0, SIGMA_OUT);
    cvSmooth(cur, g2, CV_GAUSSIAN, 5, 0, SIGMA_IN);
```

```
        cvAbsDiff(g1, g2, cur);
        cvConvertScale(cur, cur, 5);

        int p1=image->widthStep/sizeof(float);
        int p2=tmp->widthStep; //uchar
        int cy = (tmp->height - height)/2;
        int cx = (tmp->width - width)/2;
        for(int x=0; x<width; x++) {
          for(int y=0; y<height; y++) {
            ((float*)image->imageData)[y*p1+x] = ( (float)(((unsigned char*)
                cur->imageData)[(cy+y)*p2+cx+x]) - (float)(((unsigned char*)
                prev->imageData)[(cy+y)*p2+cx+x]) )/255.0f;

          }
        }


      }

    }



    Layer::Layer(int w, int h, int rf, int moduleN_, float sigmaRf_, Retina
        *r) {
      this->width = w;
      this->height = h;
      this->retina = r;

      this->rf = rf;
      this->rf21 = 2*rf+1;
      this->rf2 = this->rf21*this->rf21;
```

```
this->sigmaRf = sigmaRf_;
this->sigmaRf2 = sigmaRf_*sigmaRf_;
this->gaussianAperture = (float*)malloc(this->rf2*sizeof(float));
for(int j=0; j<rf21; j++) {
  for(int k=0; k<rf21; k++) {
    int xx = j-rf;
    int yy = k-rf;
    this->gaussianAperture[k*rf21+j] = exp( -(xx*xx+yy*yy)/(2.0f*
        sigmaRf2) );
  }
}



this->moduleN = moduleN_;
this->numModulesW = this->width / this->moduleN;
this->numModulesH = this->height / this->moduleN;
if( (w%moduleN)!=0 || (h%moduleN)!=0 )
  cout<<"Warning: W/H not multiples of moduli's width!"<<endl;

this->weights = (float**)malloc(w*h*sizeof(float*));
for(int i=0; i<w*h; i++)
  weights[i] = (float*)malloc(this->rf2*sizeof(float));

this->out = (float*)malloc(w*h*sizeof(float));
this->out_exp = (float*)malloc(w*h*sizeof(float));

//initialize random weights
for(int i=0; i<w*h; i++) {
  float sum=0.0f;
  for(int j=0; j<this->rf2; j++) {
    this->weights[i][j] = rand()/((float)(RAND_MAX)+1.0f);
```

```
    }

  }

}

// Utility function: save "Layer" objects
void Layer::save(const char *file) {
  FILE *fp=fopen(file, "wb");

  writeint(width, fp);
  writeint(height, fp);

  writeint(rf, fp); //recompute rf21, rf2
  writefloat(sigmaRf, fp); //recompute sigmaRf2 + gaussianAperture
  writeint(moduleN, fp); //recompute numModulesW and H

  for(int i=0; i<width*height; i++) {
    for(int j=0; j<rf2; j++)
      writefloat(weights[i][j],fp);
  }

  fclose(fp);
}

// Load "Layer" objects
Layer::Layer(const char *file, Retina *r) { //load
  FILE *fp=fopen(file, "rb");

  readint(this->width, fp);
```

```
    readint(this->height, fp);

    readint(this->rf, fp); //recompute rf21, rf2
    this->rf21 = 2*this->rf+1;
    this->rf2 = this->rf21*this->rf21;

    readfloat(this->sigmaRf, fp); //recompute sigmaRf2 + gaussianAperture
        !!
    this->sigmaRf2 = this->sigmaRf*this->sigmaRf;
    this->gaussianAperture = (float*)malloc(this->rf2*sizeof(float));
    for(int j=0; j<rf21; j++) {
      for(int k=0; k<rf21; k++) {
        int xx = j-rf;
        int yy = k-rf;
        this->gaussianAperture[k*rf21+j] = exp( -(xx*xx+yy*yy)/(2.0f*
            sigmaRf2) );
      }
    }

    readint(this->moduleN, fp); //recompute numModulesW and H
    this->numModulesW = this->width / this->moduleN;
    this->numModulesH = this->height / this->moduleN;
    if( (this->width%this->moduleN)!=0 || (this->height%this->moduleN)!=0
        )
      cout<<"Warning: W/H not multiples of moduli's width!"<<endl;

    this->retina = r;


    this->weights = (float**)malloc(this->width*this->height*sizeof(float
        *));
    for(int i=0; i<this->width*this->height; i++)
```

```
    weights[i] = (float*)malloc(this->rf2*sizeof(float));

  this->out = (float*)malloc(this->width*this->height*sizeof(float));
  this->out_exp = (float*)malloc(this->width*this->height*sizeof(float))
      ;

  for(int i=0; i<this->width*this->height; i++) {
411   for(int j=0; j<this->rf2; j++)
      readfloat(weights[i][j],fp);
  }

  fclose(fp);
}


Layer::~Layer() {
  free(out);
421 free(out_exp);
  for(int i=0; i<width*height; i++)
    free(weights[i]);
  free(weights);
  free(gaussianAperture);

}


// Draw "Layer" weights into "weights_out" image
431 void Layer::getAllWeights(IplImage *weights_out, float amp) {
  float *f = (float*)weights_out->imageData;

  int ww = (rf21+1)*moduleN+2;
```

```
for(int x=0; x<weights_out->width; x++) for(int y=0; y<weights_out->
    height; y++) f[y*weights_out->width+x]=1.0f;

for(int x=0; x<width/moduleN; x++) {
  for(int y=0; y<height/moduleN; y++) {

441     int startX = x*moduleN;
    int startY = y*moduleN;
    for(int x2=0; x2<moduleN; x2++) {
      for(int y2=0; y2<moduleN; y2++) {
        int baseU = (startY+y2)*width+(startX+x2);


        for(int j=0; j<rf21; j++) {
          for(int k=0; k<rf21; k++) {
            int ind = j*rf21+k; // y+j  x+k
451

            f[ (y*ww + y2*(rf21+1) + j)*weights_out->width + (x*ww +
                x2*(rf21+1) + k) ] = (weights[baseU][ind])*amp/2.0f
                +0.5f;// /2.0f+0.5f;


          }
        }


      }
    }//end x2

461

  }
}
```

```
}


// Core of the simulation; learn weights
void Layer::train(int numIterations) {
  float *f = (float*)retina->image->imageData;

471

  const float eta = 0.007f;

  float wAmp = (retina->width - 2.0f*rf)/(float)width;
  float hAmp = (retina->height - 2.0f*rf)/(float)height;

  for(int iii=0; iii<numIterations; iii++) {
    if((iii%1000)==0)
      cout<<iii<<endl;

481   retina->getImage();

    // Compute activation
    for(int x=0; x<width; x++) {     //for x,y
      for(int y=0; y<height; y++) { //
        int baseU = y*width+x;

        int cx = x*wAmp;
        int cy = y*hAmp;

491     float sum = 0.0f;
        float sumx=0.0f;
        for(int j=0; j<rf21; j++) {
          for(int k=0; k<rf21; k++) {
            int ind = j*rf21+k; //y+j  x+k
```

```
            float x_i = f[ (int)(cy + j)*retina->width + (int)(cx + k)
                ];
            //x_i = x_i * gaussianAperture[ind];


            sum += x_i * weights[baseU][ind];
            sumx+=x_i*x_i;

          }
        }
        sumx=sqrt(sumx);
        if(sumx>0.0f)
          sum/=sumx;

        out[baseU] = sum;

      }
    }


    //CORE ALGORITHM!
    //Update weights!
    for(int x=0; x<width; x++) {     //for x,y
      for(int y=0; y<height; y++) { //
        int baseU = y*width+x;

        int moduleX = x/moduleN;
        int moduleY = y/moduleN;
        int startX = moduleX*moduleN;
        int startY = moduleY*moduleN;

        int cx = x*wAmp;
```

```
    int cy = y*hAmp;


531     float neigh = out[baseU];

    float mmax=0.0f;
    for(int xx=startX; xx<startX+moduleN; xx++) {
      for(int yy=startY; yy<startY+moduleN; yy++) {
        float val = out[yy*width+xx];
        if(val>mmax) mmax=val;
      }
    }
    if(neigh < mmax) neigh=-neigh/100.0f; // /170.0f;// /170.0f;
541


    for(int j=0; j<rf21; j++) {
      for(int k=0; k<rf21; k++) {
        int ind = j*rf21+k;  //y+j  x+k

        float x_i = f[ (int)(cy + j)*retina->width + (int)(cx + k)
            ];
        //x_i = x_i * gaussianAperture[ind];

        weights[baseU][ind] = weights[baseU][ind] + eta*neigh*( x_i
            - weights[baseU][ind]*neigh );
551


      }
    }


  } //
```

```
    }   //end for x,y


561  } //end numIterations

}



int main() {
  srand(time(0));

  int rf=6;
571  int rf21=2*rf+1;
  int rf2=rf21*rf21;

  int moduleN = 4;
  int W = moduleN*2;
  int H = W;

  int RetinaW = W+2*rf;
  int RetinaH = RetinaW;
  Retina *retina = new Retina(RetinaW, RetinaH, RETINA_MODE_CALTECH); //
     VIDEO - DEBUG - CALTECH
581

  float sigmaRf = 6.0f;
  Layer *layer = new Layer(W, H, rf, moduleN, sigmaRf, retina);
  //Layer *layer = new Layer("out.net", retina);

  cout<<"Width="<<W<<"   "<<"RetinaWidth="<<RetinaW<<endl;

  IplImage *outIm=cvCreateImage(cvSize(W, H), IPL_DEPTH_32F, 1);
```

```
    int WSIZE = ((rf21+1)*moduleN+2)*W/moduleN;
591 IplImage *weights_out=cvCreateImage(cvSize(WSIZE, WSIZE),
        IPL_DEPTH_32F, 1);



    layer->train(20000);
    layer->save("out.net");



    layer->getAllWeights(weights_out, 2.0f);
    cvNamedWindow("exc_final", CV_WINDOW_AUTOSIZE);
    cvShowImage("exc_final", weights_out);
601

    // Write output to image; OpenCV cannot save IPL_DEPTH_32F
    IplImage *oout = cvCreateImage(cvSize(weights_out->width, weights_out
        ->height), IPL_DEPTH_8U, 1);
    for(int x=0; x<oout->width; x++) {
      for(int y=0; y<oout->height; y++) {
        ((unsigned char*)oout->imageData)[y*oout->width+x] = (unsigned
            char)( 255.0f * ( ((float*)weights_out->imageData)[y*
            weights_out->widthStep/sizeof(float)+x] ) );


      }
    }
    cvSaveImage("weights.png", oout);
611

    cvWaitKey();


    return 0;
  }
```